Bond-Forming Reactions of Dications with Molecules: A Computational and Experimental Study of the Mechanisms for the Formation of HCF_2^+ from CF_3^{2+} and H_2†

Natalie Lambert,‡ Nikolas Kaltsoyannis,*,‡ Stephen D. Price,*,‡ Jan Žabka,§ and Zdenek Herman§

Department of Chemistry, University College London, 20 Gordon Street, London WC1H 0AJ, U.K., and V. Čermák Laboratory, J. Heyrovský Institute of Physical Chemistry, Academy of Sciences of the Czech Republic, Dolejškova 3, CZ-182 23 Prague 8, Czech Republic

Received: June 4, 2005; In Final Form: July 22, 2005

The QCISD and QCISD(T) quantum chemical methods have been used to characterize the energetics of various possible mechanisms for the formation of HCF_2^+ from the bond-forming reaction of CF_3^{2+} with H_2. The stationary points on four different pathways leading to the product combinations $HCF_2^+ + H^+ + F$ and $HCF_2^+ + HF^+$ have been calculated. All four pathways begin with the formation of a collision complex $[H_2-CF_3]^{2+}$, followed by an internal hydrogen atom migration to give $HC(FH)F_2^{2+}$. In two of the mechanisms, immediate charge separation of $HC(FH)F_2^{2+}$ via loss of either HF^+ or a proton, followed by loss of an F atom, yields the experimentally observed bond-forming product HCF_2^+. For the other two mechanisms, internal hydrogen rearrangement of $HC(FH)F_2^{2+}$ to give $C(FH)_2F^{2+}$, followed by charge separation, yields the product CF_2H^+. This product can then overcome a 2.04 eV barrier to rearrange to the HCF_2^+ isomer, which is 1.80 eV more stable. All four calculated mechanisms are in agreement with the isotope effects and collision energy dependencies of the product ion cross sections that have been previously observed experimentally following collisions between CF_3^{2+} and H_2/D_2. We find that in this open-shell system, CCSD(T) and QCISD(T) T_1-diagnostic values of up to 0.04 are acceptable. A series of angularly resolved crossed-beam scattering experiments on collisions of CF_3^{2+} with D_2 have also been performed. These experiments show two distinct channels leading to the formation of DCF_2^+. One channel appears to correspond to the pathway leading to the ground state $^1DCF_2^+ + D^+ + F$ product asymptote and the other to the $^3DCF_2^+ + D^+ + F$ product asymptote, which is 5.76 eV higher in energy. The experimental kinetic energy releases for these channels, 7.55 and 1.55 eV respectively, have been determined from the velocities of the DCF_2^+ product ion and are in agreement with the reaction mechanisms calculated quantum chemically. We suggest that both of these observed experimental channels are governed by the reaction mechanism we calculate in which charge separation occurs first by loss of a proton, without further hydrogen atom rearrangement, followed by loss of an F atom to give the final products $^1DCF_2^+ + D^+ + F$ or $^3DCF_2^+ + D^+ + F$.

I. Introduction

The bond-forming reactivity of doubly charged cations (dications) with molecules has, until recently, remained relatively unexplored. This is in large part due to the fact that the bond-forming product ions from collisions between dications and molecules are often formed with much smaller cross sections than the products of dissociative and nondissociative electron-transfer processes.[1,2] Nevertheless, by means of careful experimentation at low collision energies (~eV) and pressures (~10^{-4} Torr), an increasing number of studies of collisions of dications with molecules have reported the observation of one or more product ions involving the formation of new chemical bonds.[2−6] Indeed, some studies have even reported bond-forming reactions that generate dications.[4,7−9]

One collision system that has received particular attention is $CF_3^{2+} + X_2$ (X = H,D). The bond-forming product ion DCF_2^+ was first observed by Price et al. in 1994[2] in an experimental study of collisions of CF_3^{2+} with D_2. No F^+ or DF^+ ions were reported in this study, so the following reaction mechanism was proposed for the formation of DCF_2^+:

$$CF_3^{2+} + D_2 \rightarrow DCF_2^+ + F + D^+ \qquad (1)$$

Price et al. suggested that the mechanism for the formation of DCF_2^+ from CF_3^{2+} and D_2 perhaps involved D^- transfer from the neutral to the dication. A later study by Tafadar et al.[10] of collisions between CF_3^{2+} and HD demonstrated an intramolecular isotope effect in the formation of HCF_2^+ and DCF_2^+. This isotope effect was originally explained in terms of a preferential orientation of the reactants preceding the chemical reaction. However, Tafadar et al. also reported the observation of the HF^+/DF^+ bond-forming product ions, whose formation did not exhibit an intramolecular isotope effect. This indicated that the orientational mechanism may not be the dominant effect in the dynamics. If such a mechanism were operating, one would expect *all* products of the bond-forming reaction to exhibit an intramolecular isotope effect. In a more recent study by Tafadar et al.[11] on the reactions of CF_3^{2+} with H_2 and D_2 it was also noted that the cross sections for the formation of the XCF_2^+ and XF^+ ions had significantly different collision energy

† Part of the special issue "Jürgen Troe Festschrift".

* Corresponding authors e-mail: s.d.price@ucl.ac.uk (S.D.P.) and n.kaltsoyannis@ucl.ac.uk (N.K.).

‡ University College London.

§ Academy of Sciences of the Czech Republic.

10.1021/jp052981d CCC: $33.50
Published on Web 10/04/2005

dependencies, suggesting that XCF_2^+ and XF^+ are formed via two different mechanisms.

As the existing experimental data could not provide any additional clues as to the mechanisms for the reactions of CF_3^{2+} with X_2 to give XCF_2^+ and XF^+, it became necessary to look to computational studies for further insight. The first quantum chemical study of a potential energy surface for the gas-phase reaction between a dication and a molecule was carried out by Mrázek et al.[12] on the reaction of CO_2^{2+} with H_2 to give $HCO^+ + H^+ + O$. They calculated the stationary points on the potential energy surface of the reaction and determined a mechanism in which the CO_2^{2+} and H_2 first form a loosely associated collision complex $[H_2-CO_2]^{2+}$. Internal H-atom rearrangement then occurs to give $[HCOOH]^{2+}$ which then loses a proton and an F-atom in two separate steps to leave the products $HCO^+ + H^+ + O$. An analagous mechanism for the reaction of CF_2^{2+} with H_2 has also been determined by Hrůšak.[13]

On the basis of these results, Tafadar et al.[11] suggested that the reaction of CF_3^{2+} with X_2 may be occurring via a similar mechanism. The first step would involve the formation of an $[X_2-CF_3]^{2+}$ collision complex, followed by X-atom migration from the C to an F atom. Formation of the products $XCF_2^+ + X^+ + F$ could then occur by subsequent cleavage of an F−X bond and a C−F bond in two steps, while the formation of $XCF_2^+ + XF^+$ could occur by a simple C−F bond cleavage. Crucially, the reaction coordinate which defines the pathway for formation of X^+ is the F−X bond cleavage. Rice−Ramsperger−Kassel−Marcus (RRKM) calculations performed by Tafadar et al.[11] on the $CO_2^{2+} + X_2$ system showed that the rate for the O−D cleavage is 66% slower than for O−H cleavage, due to a greater number of accessible vibrational states at the transition state leading to H^+ loss rather than D^+ loss. The same argument could be applied for the formation of X^+ by F−X bond cleavage in the $CF_3^{2+} + X_2$ system. Of course, there would be no kinetic competition for the formation of XF^+, as the reaction coordinate of interest (C−F bond breaking) does not involve an X atom. This statistical argument was used to to explain why an isotope effect is noticed in the formation of XCF_2^+ but not XF^+ in the reaction of CF_3^{2+} with HD.[11]

There currently exist only four computational analyses of the potential energy surfaces for the reactions of dications with neutrals. In addition to the study by Mrázek et al.[12] discussed above, we recently performed a quantum chemical investigation of the potential energy surface of the reaction of CF_2^{2+} with H_2O to give $OCF^+ + H^+ + HF$.[6] These calculations revealed a mechanism analogous to that proposed by Mrázek et al. for their $CO_2^{2+} + H_2$ system. CF_2^{2+} and H_2O initially associate to give the $[H_2O-CF_2]^{2+}$ complex. As with the $CO_2^{2+} + H_2$ system, this is followed by internal H-atom rearrangement to give $[HO-CF_2H]^{2+}$. This complex then loses a proton and finally the HF molecule in two distinct steps to give the products. This mechanism was later confirmed by a series of crossed-beam coincidence experiments, in which the dynamics and kinematics of such three-body reactions can be fully monitored on a per-event basis.[5] More recent computational studies have also been performed on the systems $CHCl^{2+} + H_2$[14] and $Ar^{2+} + NH_3$.[15] As with the mechanisms described above, these reactions also take place via one or more collision complexes.

In this paper we describe the results of a series of ab initio calculations on the important features of the potential energy surface for the reaction between CF_3^{2+} and H_2. These calculations reveal four primary pathways to the formation of the experimentally observed products. We find that these mechanisms support the explanation suggested by Tafadar et al.[10] for the observed isotopic effects. In addition, we present the results of a series of angularly resolved crossed-beam scattering experiments between CF_3^{2+} and D_2. Two distinct pathways are observed. Both correspond well with the energetics of the reaction mechanisms we have calculated quantum chemically.

II. Computational Details

Although other approaches were attempted (as discussed in the main text), the ab initio quadratic configuration interaction singles and doubles (QCISD) method was selected for the full characterization of the stationary points along the potential energy surfaces for the bond-forming reactions of CF_3^{2+} and H_2 to give either $HCF_2^+ + H^+ + F$ or $HCF_2^+ + HF^+$. The 6-311G(d,p) basis set was used for all production calculations. Geometry optimizations were performed at the QCISD level, followed by frequency calculations in order to characterize each stationary point and to obtain the zero-point energy. Single-point calculations were then performed on each of the optimized geometries at the QCISD(T) level in order to refine the energies of each structure.

Intrinsic reaction coordinate (IRC) calculations using QCISD were performed along the reactive mode corresponding to the imaginary frequency of each transition state to verify the connectivity of all minima and saddle points. Where necessary, restricted geometry optimizations were performed in order to map out certain problematic regions of a surface. The *Gaussian03* program was used for all calculations.[16]

III. Experimental Details

Crossed-beam collision experiments between CF_3^{2+} and D_2 were performed using the EVA II apparatus, which has been described in detail before.[17] Briefly, CF_3^{2+} dications are formed in a low-pressure source by electron ionization of CF_4 using 130 eV electrons. The products of the ionization are extracted from the source, the CF_3^{2+} dications are mass selected, and the resulting dication beam is decelerated to the required laboratory collision energy (∼eV). This dication beam has a typical energy spread of 0.2−0.5 eV and an angular spread of about 1° at full width half-maximum (fwhm). The neutral reactant beam is then introduced from a multichannel jet at a right angle to the dication beam and with an angular spread of 10° fwhm. The products of the collision pass through a detection slit into a stopping-potential energy analyzer and are then accelerated and focused into a detection mass spectrometer for mass analysis. Finally the products are detected using a dynode electron multiplier. To correct for background scattering, the neutral reactant beam is modulated using a beam chopper, and phase sensitive detection and signal averaging are used. The angular distributions of the products following the collision were obtained by rotating both the dication and neutral beams with respect to the collision center. In the present case the intensity of the DCF_2^+ product ion was rather low. Hence, instead of a full scattering diagram, only energy profiles at a scattering angle close to the angular maximum could be determined for this ion.

IV. Results and Discussion

A. Computational Results. *A.1. Ab initio versus DFT Methods and the T1-Diagnostic.* The stationary points along a number of pathways on the potential energy surface (PES) for the bond-forming reaction of CF_3^{2+} with H_2 were first optimized using the B3LYP hybrid DFT method with the 6-311G(d,p) Pople style basis set. Four distinct pathways were found leading to the formation of the bond-forming product ion, HCF_2^+. Three key barrier heights for the dominant reactive

pathway were recalculated at the B3LYP level using the larger 6-311++G(2df,2pd) basis set. Differences in these three barrier heights between those calculated at the B3LYP/6-311G(d,p) level and those calculated at the B3LYP/6-311++G(2df,2pd) level were all less than 0.06 eV. Therefore the extra diffuse and polarization functions were omitted from subsequent calculations in order to save computational time. It is unsurprising that diffuse functions are not required to satisfactorily model systems with one or more positive charges.

Single-point energy calculations were then performed on the B3LYP-optimized geometries using the CCSD(T) method and the 6-311G(d,p) basis set. The T_1-diagnostic was also evaluated for each point using CCSD(T). The T_1-diagnostic of Lee and Taylor[18] is a measure of the weighting of the single excitations in the cluster operator

$$T_1 = \sqrt{\frac{\sum_{i}^{\text{occ}}\sum_{a}^{\text{vir}}(t_i^a)^2}{n}} \qquad (2)$$

where t_i^a is the amplitude of single excitations from occupied orbital i to virtual orbital a, and n is the number of electrons. The T_1-diagnostic is often used as a qualitative estimate of the degree of multireference character of a system. A value of 0.02 for the T_1-diagnostic was suggested by Lee and Taylor as a threshold above which the reliability of single reference methods would become questionable.[18] However, they also noted that the threshold may well be higher for open-shell systems. Since then, a number of studies have shown that T_1-diagnostic values of up to 0.045 may be acceptable in open-shell systems.[18−21] The T_1-diagnostic values calculated for the stationary points in our system lay between 0.018 and 0.027. Although these fall below the open-shell threshold of 0.045, we felt it would be useful to compare our B3LYP-optimized PESs with those calculated by a different method, ideally one which recovers more dynamic electron correlation.

The obvious method to use in order to include possible multireference effects is the multireference configuration interaction (MRCI) method. We first attempted to perform geometry optimizations at the complete-active-space self-consistent field (CASSCF) level using a full valence active space and the cc-pvtz basis set using the Molpro2002 code.[22] For our largest structures, a full valence active space consisted of 15 electrons in 13 orbitals. However, it soon became clear that such active spaces would not be sufficient for a meaningful investigation of the potential energy surface as there existed many energetically near-degenerate orbitals of similar character at the active space limit. Since we were investigating a reaction pathway which involves many different reactive coordinates, it would have been necessary to include orbitals relevant to all of these coordinates. Unfortunately, such an enlargment of the active space was not computationally feasible.

We subsequently decided to make use of the QCISD method in order to investigate the PES. Although a single reference method, QCISD is a high level ab initio approach that recovers much dynamic correlation and a good deal of nondynamic correlation as well. QCISD is size-consistent and has a reasonably efficient implementation of analytic gradients and numerical frequencies in the *Gaussian03* program.[16] Stationary point geometries, zero-point energies, vibrational frequencies, and IRC calculations were all performed using QCISD and the 6-311G(d,p) basis set. QCISD(T)/6-311G(d,p) single-point energies and Q_1-diagnostics were then evaluated on the optimized geometries.

TABLE 1: Comparison of Barrier Heights for Each Activation Step in All Four Calculated Pathways, as Determined by B3LYP and QCISD(T)//QCISD Methods[a]

pathway	B3LYP	QCISD(T)//QCISD	difference
		Proton Loss 1	
barrier 1	0.60	0.61	0.01
barrier 2	1.40	1.54	0.14
barrier 3	0.76	0.91	0.15
		HF + Loss 1	
barrier 1	0.60	0.61	0.01
barrier 2	0.04	0.17	0.13
		Proton Loss 2	
barrier 1	0.60	0.61	0.01
barrier 2	0.87	0.75	−0.12
barrier 3	1.22	1.70	0.49
barrier 4	3.15	2.81	−0.32
		HF + Loss 2	
barrier 1	0.60	0.61	0.01
barrier 2	0.87	0.75	−0.12
barrier 3	0.54	0.76	0.22

[a] Barrier heights and differences are given in eV. Barrier numbers are given in the order in which they are encountered in the reaction mechanism.

TABLE 2: Bond Lengths for All Calculated (QCISD) Structures[a]

symbol	structure	H−C/Å	H−F/Å	C−F/Å
I	$H_2CF_3^{2+}$	1.47[2]		1.36[2],1.22
II	$H_2CF_3^{2+}$ TS	1.22	1.48	1.35[2],1.30
III	$HC(FH)F_2^{2+}$	1.42	1.86	1.23[2],1.51
IV	$HC(FH)F_2^{2+}$ TS	1.43	1.91	1.25[2],1.34
V	HCF_3^{+}	2.74		1.23[3]
VI	HCF_3^{+} TS	1.14		1.25]2],1.60
VII	HCF_2FH^{2+} TS	1.33	0.97	1.21[2],1.79
VIII	$HC(FH)F_2^{2+}$ TSb	1.43	0.99	1.22,1.35.1.48
IX	$C(FH)_2F^{2+}$		0.98[2]	1.50[2],1.21
X	$C(FH)_2F^{2+}$ TS		1.95,0.95	1.23,1.64,1.31
XI	CF_3H^{+}		0.94	1.24[2],1.89
XII	CF_3H^{+} TS		0.92	1.17,2.17,1.96
XIII	CF_2HFH^{2+}		0.96,0.98	1.17,1.57,1.86
	CF_3^{2+}			1.18[2], 1.55
	H_2	0.74 (H−H)		
	$^1HCF_2^{+}$	1.09		1.23[2]
	$^3HCF_2^{+}$	2.88		1.22[2]
	HF^{+}		0.99	
	F			
	CF_2H^{+} TS	1.33		1.45,1.21
	CF_2H^{+}		0.92	1.17,2.19

[a] The symbols in the first column refer to labels used in Figures 1−4. Numbers in square brackets indicate the number of degenerate bond lengths. No symmetry constraints were imposed during any of the geometry optimizations.

The Q_1-diagnostic is the QCISD equivalent[23] of the coupled cluster T_1-diagnostic, and the same thresholds for the suitability of single reference methods apply (i.e. 0.020 for closed shell and 0.045 for open shell systems).

The same four pathways as evaluated at the B3LYP level were found and are shown in Figures 1−4. The general shapes of the surfaces calculated at the QCISD(T)//QCISD level are not significantly different from those calculated at the B3LYP level. As can be seen from the relative barrier heights given in Table 1, the largest difference in activation energies between the two methods is 0.49 eV. Most of the geometries of the stationary points remained very similar as well. The geometric parameters for each stationary point calculated at the QCISD level are given in Tables 2 and 3. The total energies, zero-point energies, and Q_1-diagnostics for each stationary point are given in Table 4.

TABLE 3: Bond Angles for All (QCISD) Calculated Structures[a]

symbol	structure	H−C−F	F−C−F	H−F−C
I	$H_2CF_3^{2+}$	93.6[2],108.4	120.7[2],91.1	
II	$H_2CF_3^{2+}$ TS	112.6[2],108.7	116.5[2],92.0	
III	$HC(FH)F_2^{2+}$	102.1,104.8,98.0	127.5,112.3,107.5	124.4
IV	$HC(FH)F_2^{2+}$ TS	99.7[2],100.7	115.0[2],121.2	161.3
V	HCF_3^{+}	90.4[3]	120.0[3]	
VI	HCF_3^{+} TS	117.2[2],78.1	109.2,117.9	
VII	HCF_2FH^{2+} TS	113.6,71.7,111.3	129.9,111.0,103.3	127.7
VIII	$HC(FH)F_2^{2+}$ TSb	57.0,131.3,112.0	122.1,105.1,114.0	122.9
IX	$C(FH)_2F^{2+}$		98.0,112.0,111.1	120.5[2]
X	$C(FH)_2F^{2+}$ TS		107.9,100.9,117.7	119.5,164.3
XI	CF_3H^{+}		102.4[2],120.4	119.7
XII	CF_3H^{+} TS		91.3,99.6,112.1,99.6	136.2
XIII	CF_2HFH^{2+}		108.0,135.1,116.8	120.9,124.7
	CF_3^{2+}		110.1[2],139.9	
	H_2			
	$^1HCF_2^{+}$	120.8[2]	118.4	
	$^3HCF_2^{+}$	93.9[2]	124.9	
	HF^{+}			
	F			
	CF_2H^{+} TS	50.5,161.5	111	
	CF_2H^{+}	-	90.6	138.6

[a] The symbols in the first column refer to labels used in Figures 1−4. Numbers in square brackets indicate the number of degenerate bond angles. No symmetry constraints were imposed during any of the geometry optimizations. All bond angles are given in degrees.

TABLE 4: Total Energies, Zero-Point Energies, Zero-Point Corrected Energies, and Q_1-Diagnostics for All Structures[a]

symbol	structure	total energy	zero-point energy	zero-point corrected energy	Q_1-diagnostic
I	$H_2CF_3^{2+}$	−336.9437745	0.024572	−336.9192025	0.0269
II	$H_2CF_3^{2+}$ TS	−336.9204905	0.023915	−336.8965755	0.0260
III	$HC(FH)F_2^{2+}$	−337.0701787	0.026513	−337.0436657	0.0209
IV	$HC(FH)F_2^{2+}$ TS	−337.0069378	0.019647	−336.9872908	0.0200
V	HCF_3^{+}	−337.1512063	0.019647	−337.1315593	0.0180
VI	HCF_3^{+} TS	−337.1196899	0.020914	−337.0987759	0.0199
VII	HCF_2FH^{2+} TS	−337.0637402	0.026115	−337.0376252	0.0167
VIII	$HC(FH)F_2^{2+}$ TSb	−337.0409327	0.024630	−337.0163027	0.0402
IX	$C(FH)_2F^{2+}$	−337.1160944	0.028492	−337.0876024	0.0245
X	$C(FH)_2F^{2+}$ TS	−337.0467039	0.021636	−337.0250679	0.0195
XI	CF_3H^{+}	−337.1779872	0.020600	−337.1573872	0.0196
XII	CF_3H^{+} TS	−337.0691993	0.015317	−337.0538823	0.0259
XIII	CF_2HFH^{2+}	−337.0860712	0.026682	−337.0593892	0.0227
	CF_3^{2+}	−335.7432934	0.011825	−335.7314684	0.0229
	H_2	−1.1683403	0.010068	−1.1582723	0.0058
	$^1HCF_2^{+}$	−237.5770649	0.021021	−237.5560439	0.0200
	$^3HCF_2^{+}$	−237.3732153	0.012931	−237.3602843	0.0228
	HF^{+}	−99.704935	0.006871	−99.698064	0.0069
	F	−99.5658041			0.0034
	CF_2H^{+} TS	−237.4278733	0.012884	−237.4149893	0.0239
	CF_2H^{+}	−237.5060605	0.016074	−237.4899865	0.0192

[a] All energies are given in Hartrees. Zero-point energies were calculated at the QCISD/6-311G(d,p) level. Total energies and Q_1-diagnostics were calculated at the QCISD(T) level.

Although most of the geometries of the stationary points calculated at the QCISD level were virtually unchanged from those calculated at the B3LYP level, a large difference was noticed for the HCF_3^{+} (structure V, Figure 1) ion. The largest differences were in the H−C bond length (1.32 Å at B3LYP and 2.74 Å at QCISD) and the F−C−F−F dihedral angle (144.7° at B3LYP and 178.7° at QCISD). Both structures are $^2A_1$ states. The difference in the B3LYP single point energies calculated for each structure is only 0.24 eV, and the difference in the QCISD single point energy between the two structures is 0.25 eV. A geometry optimization was performed on this ion using the coupled cluster singles and doubles (CCSD) method, and the same structure as that determined using QCISD was obtained. Given that, in general, post-Hartree−Fock methods such as CCSD and QCISD are likely to be more accurate than B3LYP, we tend to favor the ab initio geometry for structure HCF_3^{+}.

It should also be noted that all attempts to optimize the geometry of the CF_3H^{+} transition state (structure XII, Figure 3) directly were unsuccessful using QCISD. Thus, a potential energy surface scan was performed in which the optimized CF_3H^{+} minimum (XI) was used as a starting structure and the C− F bond distance was held fixed over a series of increasing values, while all other parameters were allowed to optimize. The structure at the point of maximum energy was taken as the starting guess for a QCISD transition state geometry optimization and frequency calculation. Although the geometry optimization was successful, the frequency calculation yielded three imaginary modes, the largest of which corresponds to the required C−F bond breaking (the other two modes correspond to H−C−F bend and twist). Given our lack of success with other calculations in this area of the PES, we have decided to present structure XII as our best estimate of the C−F bond

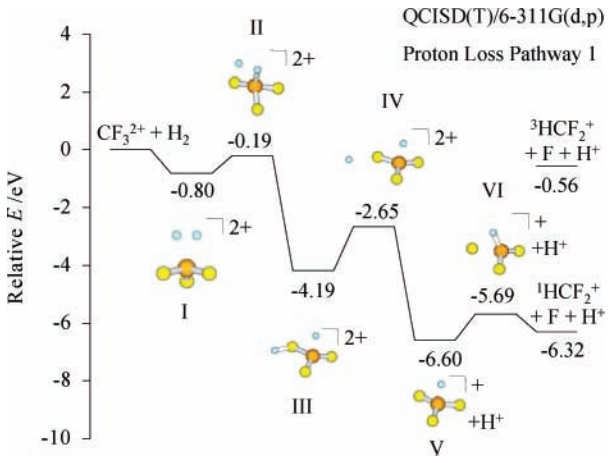

Figure 1. Calculated stationary points on one pathway on the potential energy surface for the reaction $CF_3^{2+} + H_2 \rightarrow HCF_2^+ + H^+ + F$. This pathway involves proton loss following complexation and is referred to in the text as PL1 (proton loss 1).

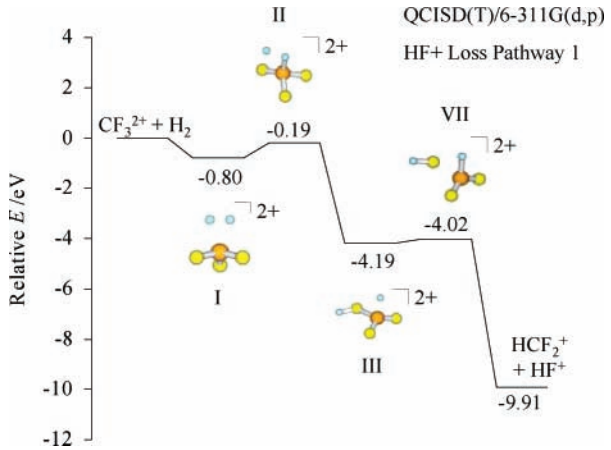

Figure 2. Calculated stationary points on one pathway on the potential energy surface for the reaction $CF_3^{2+} + H_2 \rightarrow HCF_2^+ + HF^+$. This pathway involves loss of HF^+ following complexation and is referred to in the text as HFL1 (HF^+ loss 1).

breaking transition state. A single-point QCISD(T) calculation was then also performed on this structure.

The Q_1-diagnostics for each of the calculated stationary points are shown in Table 4 and, bar one, lie in the range 0.017−0.027. The largest Q_1-diagnostic value (for structure VIII) is 0.040, still within the suggested threshold of 0.045 for open-shell systems. Given that we find good agreement between the B3LYP and QCISD methods with regards to the shapes of the potential energy surfaces and the geometries of the stationary points, it would indeed appear that T_1- and Q_1-diagnostic values of greater than 0.02 can be acceptable for open shell systems, as suggested previously.[19−21,24]

A.2. Calculated Reaction Mechanisms. As can be seen in Figures 1−4, all four pathways we determined proceed via the same initial three stationary points. First, CF_3^{2+} and H_2 associate to form the $H_2CF_3^{2+}$ (structure I) dication complex, followed by an internal H-atom rearrangement via a transition state (structure II) to give $HC(FH)F_2^{2+}$(structure III). In two of the pathways, the $HC(FH)F_2^{2+}$ complex then fragments immediately. This fragmentation occurs either via the loss of a proton followed by an F atom via two transition states to give the products $HCF_2^+ + H^+ + F$ (this pathway is called proton loss 1 (PL1) in Figure 1) or by simply losing an HF^+ molecule, again via a transition state, yielding the products $HCF_2^+ + HF^+$ (called HF^+ loss 1 (HFL1) in Figure 2).

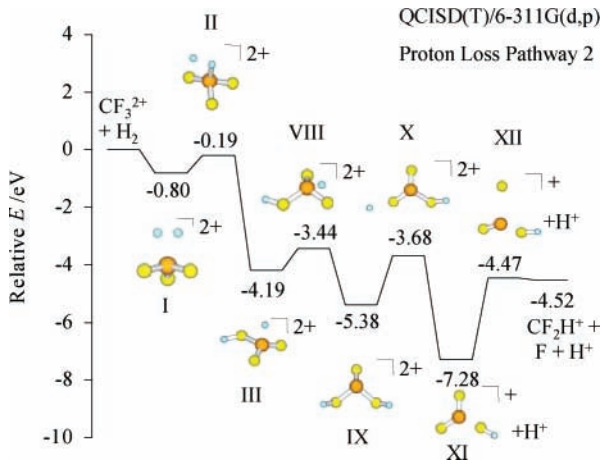

Figure 3. Calculated stationary points on one pathway on the potential energy surface for the reaction $CF_3^{2+} + H_2 \rightarrow HCF_2^+ + H^+ + F$. Like the PL1 pathway, this pathway also involves proton loss following complexation. However, an extra rearrangement step takes place before the fragmentation. This pathway is referred to in the text as PL2 (proton loss 2).

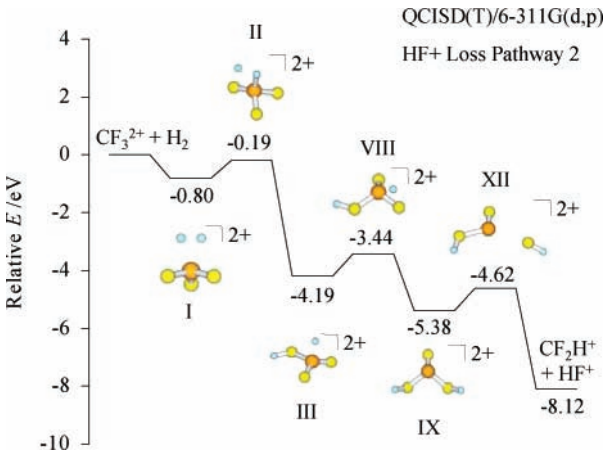

Figure 4. Calculated stationary points on one pathway on the potential energy surface for the reaction $CF_3^{2+} + H_2 \rightarrow HCF_2^+ + HF^+$. Like the HFL1 pathway, this pathway involves loss of HF^+ following complexation. However, an extra rearrangement step takes place before the fragmentation. This pathway is referred to in the text as HFL2 (HF^+ loss 2).

The two other pathways require the $HC(FH)F_2^{2+}$complex to undergo another H-atom rearrangement before fragmentation occurs. This involves the migration of the H atom from the carbon in structure III to an available fluorine via a transition state (structure VIII) to give $C(FH)_2F^{2+}$ (structure IX). One pathway then continues by loss of a proton and then an F atom (proton loss 2 (PL2) in Figure 3) to give $CF_2H^+ + H^+ + F$, and the other proceeds by the loss of an HF^+ molecule (HF^+ loss 2 (HFL2) in Figure 4) to give $CF_2H^+ + HF^+$. All of these fragmentations, as with the first two pathways, proceed via transition states. If the energy is available, the CF_2H^+ product can then overcome a 2.04 eV barrier in order to rearrange to HCF_2^+, which is 1.80 eV more stable (note that this final rearrangement is not shown in Figures 3 and 4).

One would expect that the PL1 pathway would dominate the formation of $HCF_2^+ + H^+ + F$, as the largely exothermic charge separation occurs earlier in the mechanism than in the PL2 pathway. In addition, following charge separation, the barrier for the final neutral loss step is higher for PL2 than for PL1 (2.81 eV versus 0.91 eV, repectively). If one assumes a loss of 6 eV of internal energy in the form of kinetic energy upon

charge separation, the internal energy of the CF_3H^+ complex in the PL2 pathway (structure XI) may well then not be enough to overcome this final neutral loss barrier, and the CF_3H^+ complex may instead fragment to different products and not contribute to the formation of CF_2H^+.

One would also expect that the formation of the $HCF_2^+ + HF^+$ products would be governed by the HFL1 pathway rather than HFL2, again due to charge separation occurring earlier in the mechanism. HFL1 is indeed the mechanism discussed in the Introduction, which was suggested by Tafadar et al.[11] As noted in the Introduction, such a mechanistic pattern, involving complex formation followed by rearrangement and then fragmentation, has been seen before for the bond-forming reactions of $CO_2^{2+} + H_2$,[12] $CF_2^{2+} + H_2$[13], and $CF_2^{2+} + H_2O$.[6] As predicted by Tafadar et al., X^+ formation is governed by the cleavage of an F−X bond, whereas the critical bond for XF^+ formation is C−F. This explains why an H/D isotope effect is observed for the formation of X^+ but not XF^+. In addition, our calculations show that H^+ and HF^+ are formed via different pathways. This would explain why different collision energy dependencies have been observed experimentally for the formation of H^+ and HF^+.[10,11]

Finally, to provide rationalization for the fact that the experimental ion intensities of XF^+ are approximately 5% of that of the XCF_2^+ ion, a series of vibrational Rice−Ramsperger−Kassel−Marcus (RRKM) calculations were performed in order to obtain rate constants for the fragmentation of the $HC(FH)F_2^{2+}$ ion (structure III). The methodology of these calculations is described in detail in a review article by Baer and Mayer.[25] Briefly, considering only vibrational states, the density of states of the $HC(FH)F_2^{2+}$ ion (structure III) at the required internal energy is directly computed using its harmonic vibrational frequencies derived from our electronic structure calculations and the direct counting algorithm of Beyer and Swinehart.[26] Similarly, the number of accessible vibrational states of the relevant transition state at the same internal energy is also evaluated using the calculated vibrational frequencies for these stationary points. From the ratio of the number of accessible vibrational states at the transition state to the density of initial vibrational states in the intermediate we can calculate the rate constant for the dissociation process. These calculations showed that over a range of collision energies between 0.1 and 3.0 eV, the rates for the fragmentation of $HC(FH)F_2^{2+}$ via proton loss are 15−20 times faster than via HF^+ loss. In addition to the above kinetic arguments, it has been shown previously[10] that product ions that are backward-scattered in the center-of-mass frame may be detected less efficiently in the crossed-beam experiments of Tafadar et al. The dynamics of the fragmentation of the $HC(FH)F_2^{2+}$ ion to HCF_2^+ and HF^+ are not known. However, if HF^+ is predominantly backscattered in the center-of-mass frame, this would also contribute to the very weak HF^+ product ion intensities observed experimentally. Thus, the difference in the experimentally determined intensities of HF^+ and HCF_2^+ may involve apparatus factors as well as reflecting the preferential fragmentation of the collision complex.

B. Experimental Results. A series of crossed-beam experiments has been performed to study collisions between CF_3^{2+} and D_2 at a center-of-mass collision energy of 1.16 eV. The products observed were CF_3^+, CF_2^+, DCF_2^+, D^+, and CF_2^{2+}. No DF^+ signal was detected, presumably because the sensitivity of the apparatus was not sufficient to record the weak signal of this product kinematically expected to recoil mostly into the region of laboratory angles higher than 90°, inaccessible to the experiment. In earlier experiments, Tafadar et al. have shown

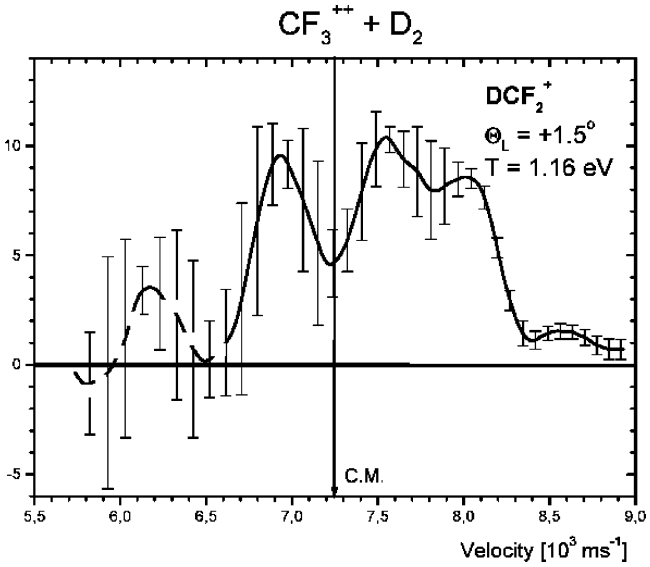

Figure 5. Velocity distribution for the DCF_2^+ product ion at a collision energy of 1.16 eV and scattering angle of $\Theta = 1.5°$. See Figure 6 for the Newton diagram that correlates with this velocity distribution.

that DF^+ was formed from $CF_3^{2+} + D_2$ collisions in very small amounts.[11] Two main channels observed experimentally leading to products involve the formation of CF_3^+ (20% of the total amount of products at $T = 1.16$ eV) and CF_2^+ (65% at $T = 1.16$ eV) and correspond to nondissociative (eq 3) and dissociative (eq 4) charge transfer.

$$CF_3^{2+} + D_2 \rightarrow CF_3^+ + D_2^+ \quad (3)$$

$$CF_3^{2+} + D_2 \rightarrow CF_3^{+*} + D_2^+ \rightarrow CF_2^+ + F + D_2^+ \quad (4)$$

Details of the scattering study of the electron-transfer process (eq 3) will be published separately. Since no F^+ ions were observed experimentally, we conclude that collision-induced charge separation does not contribute significantly to the formation of CF_2^+. It is also clear that the product dication CF_2^{2+} results from collision-induced neutral loss of CF_3^{2+}. This collision-induced neutral loss reaction is often observed in other collision systems involving CF_3^{2+}.[12]

The weakest channel detected corresponds to the formation of the product ion DCF_2^+ (15% of the total amount of products at $T = 0.72$ eV, 7% at $T = 2.09$ eV). Repeated measurements of the energy distribution of this ion product at $T = 1.16$ eV and a laboratory scattering angle $\Theta = 1.50°$ (close to the angular maximum) led to the DCF_2^+ product ion velocity distribution shown in Figure 5. This velocity distribution is plotted in the framework of the respective Newton diagram in Figure 6. Unfortunately, a full scattering diagram could not be measured due to the low intensity of the product ion.

As can be seen from Figures 5 and 6, the velocity distribution is characterized by a strong forward-scattered peak corresponding to a DCF_2^+ center-of-mass velocity of 750 m/s. There is also a second channel that exhibits symmetrical forward−backward scattering with peaks at a center-of-mass velocity of 340 m/s (see the respective circles in Figure 6). In addition, there is a small forward-scattered intensity at about 1320 m/s and a backward-scattered intensity at about 1000 m/s. However, this backward scattered intensity is buried in a large scatter of data (see Figure 5) and can be presumably regarded as an overlapping weak backward component of the two forward-scattered peaks at 750 and 1320 m/s.

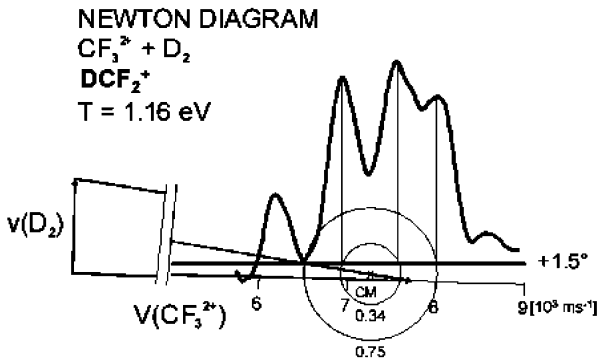

Figure 6. Newton diagram for the scattering velocities of the DCF_2^+ product ion following collisions of CF_3 with D_2 at a collision energy of 1.16 eV. The velocity distribution superimposed on the diagram is that shown in Figure 5 and was taken at a scattering angle of $\Theta = 1.5°$.

The conversion of the velocities corresponding to peaks in the DCF_2^+ velocity distribution into translational energy releases that we can compare with the values we derive from our quantum chemical calculations depends on the mechanism governing the formation of DCF_2^+. For example, to produce a DCF_2^+ ion of a given velocity, a mechanism that involves fragmentation to $DCF_2^+ + DF^+$ will release a different amount of kinetic energy than a mechanism that involves the formation of $DCF_2^+ + D^+ + F$. Below we calculate the different kinetic energy releases from our experimental DCF_2^+ velocities and compare these with the energetics predicted by our calculated PESs in order to determine the most likely reaction pathway.

B.1. DCF_2^+ 750 ms^{-1} Center-of-Mass Velocity. In this section we consider the possible pathways for forming DCF_2^+ following collisions of CF_3^{2+} with D_2 and, within the constraints of those mechanisms, convert the center-of-mass velocity of the DCF_2^+ we record experimentally into a KER to compare with previous studies of such energy releases and with the release we calculate from our PESs.

(a) Fragmentation to $DCF_2^+ + F^+ + D$. The F^+ ion has not been detected in the current, or any previous, studies of collisions of CF_3^{2+} with D_2. Hence, this pathway cannot be a significant source of DCF_2^+.

(b) $DCF_2^+ + DF^+$. This is a two-body reaction, and the corresponding KER we calculate from the velocity of DCF_2^+ is 0.53 eV. This corresponds simply to the charge separation of $D_2CF_3^{2+}$ to DCF_2^+ and DF^+:

$$CF_3^{2+} + D_2 \rightarrow D_2CF_3^{2+} \rightarrow DCF_2^+ + DF^+ \qquad (5)$$

This value of the KER appears unreasonably small, as a typical KER for the charge separation of a dication is approximately 7 eV.[1]

(c) $DCF_2^+ + D^+ + F$. To calculate the KER for the pathway that leads to these products, we first assume that DCF_2^+ is formed by loss of an F atom from DCF_3^+ following charge separation of $D_2CF_3^{2+}$ to $DCF_3^+ + D^+$. A similar pathway has been observed recently by Hu et al.[27] for the reaction of CF_3^{2+} + Ar to give $CF_2^+ + Ar^+ + F$:

$$CF_3^{2+} + D_2 \rightarrow D_2CF_3^{2+} \rightarrow DCF_3^+ + D^+ \rightarrow DCF_2^+ + D^+ + F \qquad (6)$$

This is, in effect, the mechanism PL1 that emerges from our theoretical investigations. As with pathway (b), to convert the measured velocity into a KER we consider the charge separation of $D_2CF_3^{2+}$ to $DCF_3^+ + D^+$ and assume that the KER of the subsequent neutral loss is negligible in comparison. This assumption is well supported by experimental results from studies of the dissociative electron-transfer reactions of both CO_2^{2+} and CF_3^{2+} which show that, in analogous reactions to eq 6, the energy release of the primary charge-separation step is much larger than that of the subsequent dissociation of one of the monocations formed in this charge-separation step.[12,27] More generally, the above assumption that the energy release of the charge-separation step dominates the kinematics of the decay of $D_2CF_3^{2+}$ is perfectly reasonable given that the secondary dissociation of the monocation does not involve the large electrostatic repulsion of the primary charge-separation. Indeed, charge separating dissociations of dications typically have energy releases of the order of 7 eV, much larger than the energy releases generally associated with the dissociation of polyatomic monocations. The KER we calculate for this pathway from the velocity of DCF_2^+ is 7.55 eV, a value, as discussed above, encouragingly typical for the charge separation of a dication. This value also agrees reasonably well with the KER value we determine from the calculated pathway PL1. Given the collision energy of 1.16 eV and a total reaction exothermicity of 6.32 eV from the quantum chemical calculations, the theoretical studies indicate a total of 7.48 eV energy is available for release. This value is in excellent agreement with the KER value of 7.55 eV we determine from the experimental velocity of DCF_2^+.

There is also, in principle, the possibility that the $DCF_2^+ + D^+ + F$ products are formed via a different mechanism, i.e., complexation followed by neutral loss and then fragmentation:

$$CF_3^{2+} + D_2 \rightarrow D_2CF_3^{2+} \rightarrow D_2CF_2^{2+} + F \rightarrow DCF_2^+ + D^+ + F \qquad (7)$$

Again, assuming the energy release of the neutral loss process to be negligible in comparison with that of complexation, the KER we calculate for this mechanism from the velocity of DCF_2^+ is 4.09 eV. However, we do not expect such a mechanism to predominate for the formation of $DCF_2^+ + D^+ + F$, as small dications (such as the $D_2CF_3^{2+}$ complex) tend to favor charge separation over neutral loss.

From the results discussed above, we conclude that the PL1 mechanism leading to $DCF_2^+ + D^+ + F$ in which $D_2CF_3^{2+}$ loses a proton followed by an F atom is predominant in the formation of 750 ms^{-1} DCF_2^+ ions. The strong forward scattering of the DCF_2^+ ion formed in this way is in agreement with the overall shape of the PES for this pathway (Figure 1). Specifically, the PES exhibits relatively shallow wells and a charge separation exit barrier of about 4 eV. Thus, most of the energy available in the reaction is likely to appear as the kinetic energy of the products.

B.2. DCF_2^+ 340 ms^{-1} Center-of-Mass Velocity. The same mechanisms as those described in the previous section for reaching each product asymptote will also be considered here.

(a) $DCF_2^+ + DF^+$. The KER we calculate from the velocity of DCF_2^+ for forming $DCF_2^+ + DF^+$ via direct charge separation of a collision compex (pathway 5) is 0.1 eV. Again, with such a small KER value, it is unlikely that this pathway is governing the formation of the 'slow' DCF_2^+.

(b) $DCF_2^+ + D^+ + F$. The KER we calculate from the velocity of DCF_2^+ that corresponds to the formation of 'slow' DCF_2^+ via pathway 6 is 1.55 eV. Although this value is also quite small, it may correspond to the formation of DCF_2^+ in an excited state. From our quantum chemical calculations we

determine that the formation of triplet DCF_2^+ occurs with an exothermicity of 0.56 eV (see Figure 1) and is spin-allowed. Given the collision energy of 1.16 eV, the experimentally determined KER (1.55 eV) is in good agreement with the calculated energetics for such a pathway (0.56 eV calculated exothermicity + 1.16 eV COM collision energy = 1.72 eV). In this case it must be that much of the internal energy of the collision complex is used for electronic excitation of the DCF_2^+.

As described above, there is also the possibility that the $DCF_2^+ + D^+ + F$ products are formed via pathway 7 in which neutral loss occurs before charge separation. The KER we calculate from the velocity of DCF_2^+ for such a mechanism is 0.84 eV. This value does not agree as well with our quantum chemical results, and, as above, we would expect a small dicationic collison complex, such as $D_2CF_3^{2+}$, to favor charge separation over neutral loss.

It is also interesting to note that the 340 ms^{-1} DCF_2^+ signals involve both forward and backward scattering. Such signals are indicative of a slower reaction, as the complexes involved have enough time to reorient before fragmentation. The 750 ms^{-1} peak, however, is only forward-scattered, indicative of a faster process where reorientation is not possible. If indeed the 340 ms^{-1} peaks are due to the formation of DCF_2^+ in the triplet state, the slower fragmentation indicated by the experimental data may be due to a need for greater electronic reorganization in the final fragmentation step in which an F atom is lost from doublet DCF_3^+ to give triplet DCF_2^+ and F.

From the results discussed above, we tentatively propose that the 340 ms^{-1} DCF_2^+ peaks arise from the formation of DCF_2^+ in its ground triplet state, via pathway PL1, along with D^+ and F. As discussed at the end of section B.1, we believe that the 750 ms^{-1} DCF_2^+ peak corresponds to the formation of ground singlet $DCF_2^+ + D^+ + F$, also via the PL1 pathway.

V. Conclusions

Ab initio quantum chemical calculations have been performed to elucidate the stationary points on the four distinct reactive pathways discovered on the potential energy surface for the bond-forming reaction of CF_3^{2+} with X_2 (X = H,D). We find that the H^+ and HF^+ product ions are formed via two separate pathways, explaining previously observed experimental isotope effects and collision energy dependencies. The reactive mechanism for the dominant pathway leading to the formation of $HCF_2^+ + H^+ + F$ supports a general pattern of reactivity that is emerging from recent studies of the bond-forming reactions of dications with neutral molecules. This involves the initial formation of a bound collision complex between the dication and the neutral, followed by internal rearrangement and then fragmentation to products.

The QCISD ab initio calculations presented here generally agree well with comparative B3LYP and coupled cluster studies. This agreement suggests that single-reference techniques are adequate for the current systems. The T_1/Q_1-diagnostic values found, although sometimes higher than the usually accepted 0.020 upper limit, are generally well below the 0.045 value proposed for open shell systems. Our results therefore support the use of the higher value for these diagnostics in open shell cases.

A series of crossed-beam scattering experiments was also performed between CF_3^{2+} and D_2. The angular distributions of the bond-forming DCF_2^+ product ion revealed two distinct channels. The experimentally determined kinetic energy releases for both of the channels were found to be in good agreement, within the experimental sensitivity, with the calculated mechanisms leading to the product asymptotes $^1DCF_2^+ + D^+ + F$ and $^3DCF_2^+ + D^+ + F$.

Acknowledgment. We are grateful for financial support from the Leverhulme Trust, the European Union Network RTN1-1999-00254 "Generation, Stability and Reaction Dynamics of Multiply Charged Ions (MCInet) (http://www.chm.bris.ac.uk/pt/mcinet/mcihome.htm). and the U.K.'s EPSRC for computing resources under grant GR/506233/01.

References and Notes

(1) Herman, Z.; Žabka, J.; Dolejšek, Z.; Fárník. *Int. J. Mass Spec.* **1999**, *192*, 191.

(2) Price, S. D.; Manning, M.; Leone, S. R. *J. Am. Chem. Soc.* **1994**, *116*, 8673.

(3) Kearney, D. J. A.; Price, S. D. *Phys. Chem. Chem. Phys.* **2003**, *5*, 1575.

(4) Ascenzi, D.; Franceschi, P.; Tosi, P.; Bassi, D.; Kaczorowska, M.; Harvey, J. N. *J. Chem. Phys.* **2003**, *118*, 2159.

(5) Price, S. D. *Phys. Chem. Chem. Phys.* **2003**, *5*, 1717.

(6) Lambert, N.; Kaltsoyannis, N.; Price, S. D. *J. Chem. Phys.* **2003**, *119*, 1421.

(7) Tosi, P.; Lu, W.; Correale, R.; Bassi, D. *Chem. Phys. Lett.* **1999**, *310*, 180.

(8) Tosi, P.; Correale, R.; Lu, W.; Falcinelli, S.; Bassi, D. *Phys. Rev. Lett.* **1999**, *82*, 450.

(9) Lu, W.; Tosi, P.; Bassi, D. *J. Chem. Phys.* **2000**, *112*, 4648.

(10) Tafadar, N.; Kearney, D.; Price, S. D. *J. Chem. Phys.* **2001**, *115*, 8819.

(11) Tafadar, N.; Price, S. D. *Int. J. Mass Spectrom.* **2003**, *223*−*224*, 547.

(12) Mrázek, L.; Žabka, J.; Dolejšek, Z.; Hrušák, J.; Herman, Z. *J. Phys. Chem.* **2000**, *104*, 7294.

(13) Hrušák, J. personal communications 2001.

(14) Roithová, J.; Hrušák, J.; Herman, Z. *J. Phys. Chem. A* **2003**, *107*, 7355.

(15) Lambert, N.; Kearney, D.; Kaltsoyannis, N.; Price, S. D. *J. Am. Chem. Soc.* **2004**, *126*, 3658.

(16) Frisch, M. J.; Trucks, G. W.; Schlegel, H. B.; Scuseria, G. E.; Robb, M. A.; Cheeseman, J. R.; Montgomery, J. A., Jr.; Vreven, T.; Kudin, K. N.; Burant, J. C.; Millam, J. M.; Iyengar, S. S.; Tomasi, J.; Barone, V.; Mennucci, B.; Cossi, M.; Scalmani, G.; Rega, N.; Petersson, G. A.; Nakatsuji, H.; Hada, M.; Ehara, M.; Toyota, K.; Fukuda, R.; Hasegawa, J.; Ishida, M.; Nakajima, T.; Honda, Y.; Kitao, O.; Nakai, H.; Klene, M.; Li, X.; Knox, J. E.; Hratchian, H. P.; Cross, J. B.; Bakken, V.; Adamo, C.; Jaramillo, J.; Gomperts, R.; Stratmann, R. E.; Yazyev, O.; Austin, A. J.; Cammi, R.; Pomelli, C.; Ochterski, J. W.; Ayala, P. Y.; Morokuma, K.; Voth, G. A.; Salvador, P.; Dannenberg, J. J.; Zakrzewski, V. G.; Dapprich, S.; Daniels, A. D.; Strain, M. C.; Farkas, O.; Malick, D. K.; Rabuck, A. D.; Raghavachari, K.; Foresman, J. B.; Ortiz, J. V.; Cui, Q.; Baboul, A. G.; Clifford, S.; Cioslowski, J.; Stefanov, B. B.; Liu, G.; Liashenko, A.; Piskorz, P.; Komaromi, I.; Martin, R. L.; Fox, D. J.; Keith, T.; Al-Laham, M. A.; Peng, C. Y.; Nanayakkara, A.; Challacombe, M.; Gill, P. M. W.; Johnson, B.; Chen, W.; Wong, M. W.; Gonzalez, C.; Pople, J. A. *Gaussian 03, revision B.04*; Gaussian, Inc.: Pittsburgh, PA, 2003.

(17) Herman, Z. *Int. Rev. Phys. Chem.* **1996**, *15*, 299.

(18) Lee, T. J.; Taylor, P. R. *Int. J. Quantum Chem.* **1989**, *S23*, 199.

(19) Peiró-García, J.; Nebot-Gil, I. *ChemPhysChem* **2003**, *4*, 843.

(20) Peiró-García, J.; Nebot-Gil, I. *J. Comput. Chem.* **2003**, *24*, 1657.

(21) Martínez-Ávila, M.; Peiró-García, J.; Ramírez-Ramírez, V. M.; Nebot-Gil, I. *Chem. Phys. Lett.* **2003**, *370*, 313.

(22) MOLPRO is a package of ab initio programs written by Werner, H.-J.; Knowles, P. J., with contributions from Amos, R. D.; Bernhardsson, A.; Berning, A.; Celani, P.; Cooper, D. L.; Deegan, M. J. O.; Dobbyn, A. J.; Eckert, F.; Hampel, C.; Hetzer, G.; Korona, T.; Lindh, T.; Lloyd, A. W.; McNicholas, S. J.; Manby, F. R.; Meyer, W.; Mura, M. E.; Nicklass, A.; Palmieri, P.; Pitzer, R.; Rauhut, G.; Schútz, M.; Stoll, H.; Stone, A. J.; Tarroni, R.; Thorsteinsson, T.

(23) Lee, T. J.; Rendell, A. P.; Taylor, P. R. *J. Phys. Chem.* **1990**, *94*, 5463.

(24) Rienstra-Kiracofe, J. C.; Allen, W. D.; Schaefer, H. F., III *J. Phys. Chem. A* **2000**, *104*, 9823.

(25) Baer, T.; Mayer, P. M. *J. Am. Soc. Mass Spectrom.* **1997**, *8*, 103.

(26) Beyer, T.; Swinehart, D. F. *Commun. ACM* **1973**, *16*, 379.

(27) Hu, S. W. P.; Harper, S. M.; Price, S. D. *Mol. Phys.* **2005**, *103* (13), 1809−1819.